

Electron transport, penetration depth and upper critical magnetic field of ZrB_{12} and MgB_2

V.A. Gasparov, N.S. Sidorov, I.I. Zver'kova, S.S. Khassanov, and M.P. Kulakov
*Institute of Solid State Physics RAS, 142432 Chernogolovka,
 Moscow District, Russian Federation*

(Dated: today)

We report on the synthesis and measurements of the temperature dependence of resistivity, $\rho(T)$, the penetration depth, $\lambda(T)$, and upper critical magnetic field, $H_{c2}(T)$, for polycrystalline samples of dodecaboride ZrB_{12} and diboride MgB_2 . We conclude that ZrB_{12} as well as MgB_2 behave like simple metals in the normal state with usual Bloch-Grüneisen temperature dependence of resistivity and with rather low resistive Debye temperature, $T_R = 280 \text{ K}$, for ZrB_{12} (as compared to MgB_2 with $T_R = 900 \text{ K}$). The $\rho(T)$ and $\lambda(T)$ dependencies of these samples reveal a superconducting transition of ZrB_{12} at $T_c = 6.0 \text{ K}$. Although a clear exponential $\lambda(T)$ dependence in MgB_2 thin films and ceramic pellets was observed at low temperatures, this dependence was almost linear for ZrB_{12} below $T_c/2$. These features indicate *s-wave* pairing state in MgB_2 , whereas a *d-wave* pairing state is possible in ZrB_{12} . A fit to the data gives a reduced energy gap $2\Delta(0)/k_B T_c = 1.6$ for MgB_2 films and pellets, in good agreement with published data for 3D π - sheets of the Fermi surface. Contrary to conventional theories we found a linear temperature dependence of $H_{c2}(T)$ ($H_{c2}(0) = 0.15 \text{ T}$) for ZrB_{12} .

PACS numbers: 74.70.Ad, 74.60.Ec, 72.15.Gd

1. Introduction

The recent discovery of superconductivity at 39 K in magnesium diboride [1] has initiated a booming activity in condensed matter physics. This activity has raised considerable interest in a search for superconductivity in other borides [2]. Unfortunately, so far none of natural candidates MeB_2 - type diborides of light metals ($\text{Me} = \text{Li, Be, Al, Ca}$) nor any of the large number of known isostructural transition metal diborides ($\text{Me} = \text{Ti, Zr, Hf, V, Ta, Cr, Mo, U}$) have been found to be superconducting [2]. Only in nonstoichiometric compounds ($\text{MoB}_{2.5}$, $\text{NbB}_{2.5}$, Mo_2B , W_2B , $\text{BeB}_{2.75}$) superconductivity was observed [3, 4]. Note that the earlier speculation about superconductivity in TaB_2 [5] - in contradiction to other published data [2] - has been disproved by recent resistivity, susceptibility, and the specific heat measurements [6] supported by electronic structure calculations.

These results do not seem to support the application of the old idea about superconductivity in metallic hydrogen [7] to the explanation of superconductivity in MgB_2 [8]. In spite of this fact we would like to discuss some aspects of this idea. In particular, it is believed that in MgB_2 the averaged phonon frequencies (the Debye temperature in other words) would be very high due to the low mass of boron. The latter sharply increases the prefactor in the McMillan formula for T_c . Indeed, the band structure calculations have shown that electrons at the Fermi level are predominantly boron-like and the superconductivity in MgB_2 is due to graphite-type "metallic" boron sheets [8]. Furthermore, recently Eremets *et al.* observed that the semiconducting polycrystalline boron (rhombohedral β - B_{105}) transforms to a metal under high pressure and even to a superconductor at about 160 GPa [9]. The critical temperature T_c increases from 6 K to

11.2 K at raised pressure up to 250 GPa . This observation supports old idea that a route for optimizing T_c is in preparation of the boron-rich compounds even though this does not work yet for known borides.

In fact, the search of superconductivity in borides has a long history. Matthias *et al.* discovered several superconducting cubic hexa- (MeB_6) and dodecaborides (MeB_{12}) in the 60's of the last century [10]. Many other hexa- and dodecaborides ($\text{Me} = \text{Ce, Pr, Nd, Eu, Gd, Tb, Dy, Ho, Er, Tm}$) were found to be ferromagnetic or antiferromagnetic. It was suggested that the superconductivity in YB_6 and ZrB_{12} (having highest T_c of $6.5 - 7.1 \text{ K}$ and 6.03 K , respectively [3]), might be due to the hypothetical cubic metallic boron. However, a much smaller isotope effect on T_c for boron in comparison with Zr isotopic substitution suggests that the boron in ZrB_{12} serves as inert background, and this is Zr that actually is critical for superconductivity [11, 12], even though ZrB_{12} chemically contains mainly boron.

While the superconductivity in ZrB_{12} was discovered a long time ago [10], there has been little effort devoted to the study of basic superconductive properties of this dodecaboride. Only recently, the electron transport of solid solutions $\text{Zr}_{1-x}\text{Sc}_x\text{B}_{12}$ [13] as well as the band structure calculations of ZrB_{12} [14] have been reported. Understanding the electron transport properties of the cluster borides as well as the superconductivity mechanism in these compounds is very important. In this paper we attempt to address this problem. We report temperature dependent resistivity, $\rho(T)$, magnetic field penetration depth, $\lambda(T)$, and upper critical magnetic field, $H_{c2}(T)$, for polycrystalline samples of ZrB_{12} . Comparative data of the $\rho(T)$ and $\lambda(T)$ in MgB_2 thin films and pellets are also presented.

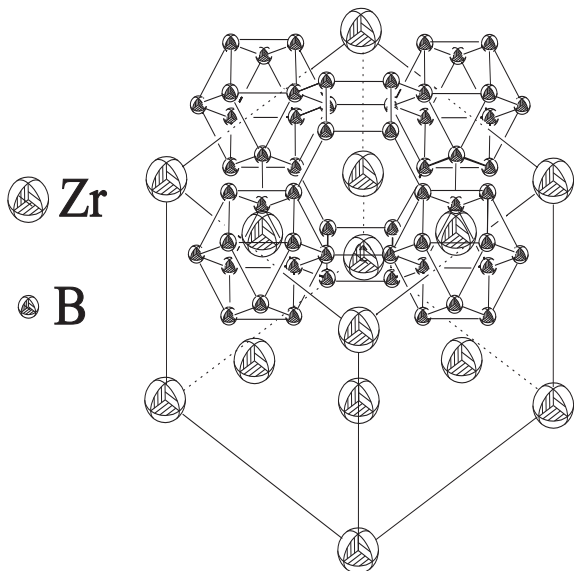


FIG. 1: The lattice structure of dodecaboride ZrB_{12} . Only B_{12} clusters on upper face of the lattice are presented for clarity.

The structure of this paper is as follows. In Sec. II we report on synthesis of ZrB_{12} and MgB_2 and the experimental techniques. Section III describes the electron transport in these compounds. Section IV describes the temperature dependence of $\lambda(T)$ in thin films and polycrystalline samples. The data on $H_{c2}(T)$ are presented in Sec. V.

II. Experimental

Under ambient conditions, dodecaboride ZrB_{12} crystallizes in the *fcc* structure (see Fig. 1) of the UB_{12} type (space group $Fm\bar{3}m$), $a = 0.7408 \text{ nm}$ [15]. In this structure, the Zr atoms are located at interstitial openings in the close-packed B_{12} clusters [13]. In contrast, the diborides show a phase consisting of two-dimensional graphite-like monolayers of boron atoms with a honeycomb lattice, intercalated with the metal monolayers [2]. In our search for superconducting diboride compounds, we observed superconductivity at 5.5 K in ZrB_2 polycrystalline samples that had a few percents amount of ZrB_{12} impurity [2]. It was recently suggested [16] that this observation could be associated with nonstoichiometry in the zirconium sub-lattice of ZrB_2 . To resolve this issue and to study the electron transport and basic superconducting properties of ZrB_{12} , we successfully synthesized this compound.

Polycrystalline samples of ZrB_{12} were obtained by conventional solid-state reaction. Starting materials were Zr metal powder (99.99% purity) and submicron amorphous boron powder (99.9% purity). These materials were lightly mixed in appropriate amounts and pressed into pellets 10 mm thick and 20 mm in diameter. The pellets were wrapped in a tungsten foil and baked at 2000°C by *e-beam* heating with subsequent slow cool-

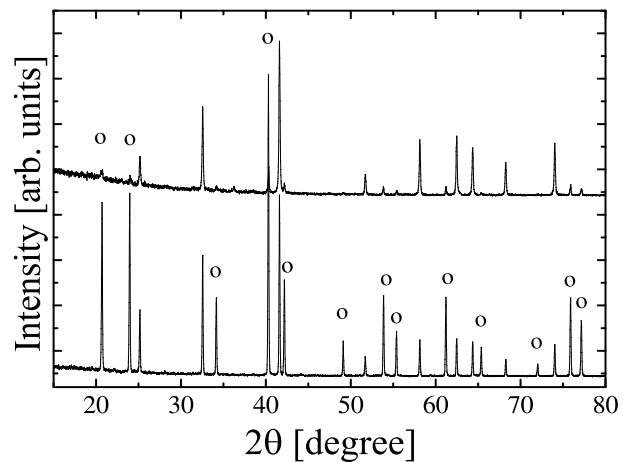


FIG. 2: Typical X-ray θ - 2θ scan of ZrB_{12} powders (lower curve), at room temperature. Similar scan for ZrB_2 pellets studied before [2] is present on upper curve. The cycles mark the X-ray reflections from *fcc* ZrB_{12} .

ing to room temperature. The process took place for two hours in a high vacuum chamber at $2 \times 10^{-4} \text{ Pa}$. The resulting polycrystalline pellets had over 90% of the theoretical mass density and were black in color. They demonstrated good metallic conductivity at low temperatures. After regrinding the prepared pellets in an agate mortar, the respective powders were reheated few times for 2 hours.

Powder X-ray diffraction pattern, obtained using $\text{CuK}\alpha$ radiation, showed that the samples largely consist of desired ZrB_{12} phase (see Fig. 2). Nevertheless, small amounts of ZrB_2 were found to be present and could not be eliminated by subsequent regrinding and annealing. A Rietveld refinement of the ZrB_{12} X-ray pattern, based on the *fcc* UB_{12} type structure presented on Fig. 1, yielded lattice parameters $a = 0.7388 \text{ nm}$ to be very close to the published values [15]. The polycrystalline MgB_2 pellets have been sintered using a similar technique as outlined in our earlier work [2]. This technique is based on the reactive liquid Mg infiltration of boron powder.

For this study, two highly crystalline, superconducting films of MgB_2 were grown on an *r*-plane sapphire substrate in a two-step process. Deposition of B precursor films via electron-beam evaporation was followed by *ex-situ* post annealing at 890°C in the presence of bulk MgB_2 and Mg vapor. Scanning electron microscopy showed dense films with surface roughness below 5 nm . For the measurements, we investigate films of 500 nm and 700 nm thick, with corresponding T_{c0} 's of 38 K and 39 K . Details about the preparation technique are described elsewhere [17].

For the resistance measurements, we used spark erosion method to cut the pellets into a rectangular bars with dimension of about $0.5 \times 0.5 \times 8 \text{ mm}^3$. The samples were lapped with diamond paste. To remove any deteriorated surface layers the samples were etched: ZrB_{12} in hot nitrogen acid, MgB_2 in 2% HCl plus water-free

ethanol, respectively. A standard four-probe *ac* (9 Hz) method was used for resistance measurements. Electrical contacts were made with Epotek H20E silver epoxy. Temperature was measured with platinum (PT-103) and carbon glass (CGR-1-500) sensors. A well-defined geometry of the samples provided for the precise resistivity measurements.

The measurements were performed in the liquid helium variable temperature cryostat in the temperature range between 1.1 K and 350 K. Magnetic measurements of the resistivity and penetration depth on the polycrystalline samples were carried out using a superconducting coil in applied fields of up to 6 T. The *dc* magnetic field was applied in the direction of the current flow. The critical temperature measured by RF susceptibility [2] and $\rho(T)$ was found to be $T_{c0} = 6.0$ K and 39.0 K for ZrB₁₂ and MgB₂ samples, respectively.

The $\lambda(T)$ dependence in thin films was investigated employing a single coil mutual inductance technique. This technique, originally proposed in [18] and improved in [19], takes advantage of the well known two-coil geometry. It was successfully used for the observation of the Berzinskii–Kosterlitz–Thouless vortex–antivortex unbinding transition in ultrathin Y₁Ba₂Cu₃O_{7-x} films [20] as well as for the study of the $\lambda(T)$ dependence for MgB₂ films [21].

In particular, this radio frequency technique measures the change of inductance ΔL of a one-layer pancake coil located in the proximity of the sample. The coil is a part of the *LC* circuit driven by a marginal oscillator operating at 2 – 10 MHz, or by the impedance meter (VM-508 TESLA 2 – 50 MHz). The frequency stability of this oscillator is 10 Hz. The film is placed at small distance (≈ 0.1 mm) below the coil and is thermally insulated from the coil by Teflon foil. Both sample and coil are in a vacuum, but the coil holder is thermally connected with helium bath, while the sample holder is isolated and may be heated. During the experiment the coil was kept at 2.5 K, whereas the sample temperature was varied from 2.5 K to 100 K. Such design allows us to eliminate possible effects in temperature changes in *L* and *C* on the measurements. The real part of the complex mutual inductance *M* between the film and the coil can be obtained through:

$$\text{Re } M(T) = L_0 \cdot \left(\frac{f_0^2}{f^2(T)} - 1 \right), \quad (1)$$

Here L_0 and f_0 are the inductance and the resonant frequency of the circuit without the sample. In the London regime, where the high frequency losses are negligible, one can introduce the difference between temperature dependant real part of *M* of the coil with the sample, $\text{Re } M(T)$, and that of the coil at T_0 $\text{Re } M_0$. This difference is a function of the $\lambda(T)$:

$$\Delta \text{Re } M(T) = \pi \mu_0 \cdot \int_0^\infty \frac{M(q)}{1 + 2q\lambda \coth(d/\lambda)} dq, \quad (2)$$

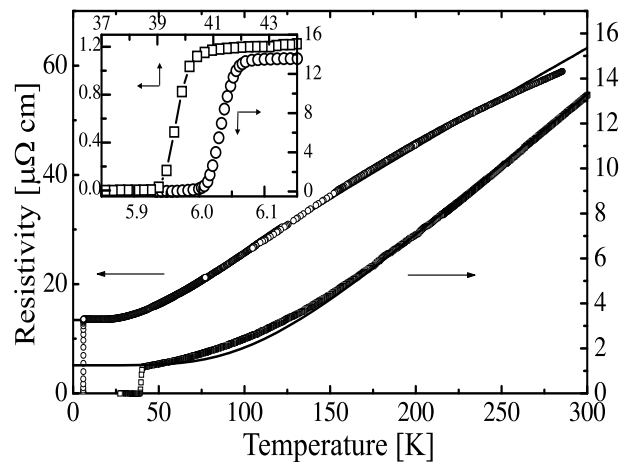


FIG. 3: Temperature dependence of the resistivity $\rho(T)$ of ZrB₁₂ (open circles) and MgB₂ (squares) polycrystalline samples. The solid lines represent BG fits to the experimental data by Eq. (4).

where $M(q)$ plays the role of mutual inductance at a given wave number q in the film plane and depends on the sample-coil distance, d is the sample thickness (additional details can be found in [19]). A change in $\Delta \text{Re } M(T)$ is detected as a change of resonant frequency $f(T)$ of the oscillating signal. This change when put into Eq. (2) yields temperature dependent London penetration depth $\lambda(T)$.

Measurements of $\lambda(T)$ for polycrystalline ZrB₁₂ and MgB₂ samples were performed with a similar *LC* technique but using a rectangular solenoid coil into which the sample was placed. The details of this technique are described elsewhere [22]. For such arrangements, changes in the resonant frequency of the circuit $f(T) = \omega/2\pi$ relative to that above T_c , $f(T_c)$, and at minimal temperature T_1 , $f(T_1)$, are directly related to the inductance of the probe coil and, hence, to $\lambda(T)$ by following equation:

$$\lambda(T) - \lambda(T_1) = \delta \cdot \frac{f^{-2}(T) - f^{-2}(T_1)}{f^{-2}(T_c) - f^{-2}(T_1)} \quad (3)$$

Here $\delta = (c^2 \rho / 2\pi \omega)^{1/2}$ is the skin depth above T_c , which was determined from the resistivity $\rho(T)$ measurements.

III. Electron Transport

Figure 3 shows the temperature dependence of the resistivity for ZrB₁₂ and MgB₂ samples. Inset displays variation of $\rho(T)$ near superconducting transition with zero resistance at 6.0 K (the width $\Delta T = 0.04$ K) in ZrB₁₂ and at 39 K ($\Delta T = 0.7$ K) in MgB₂ samples. The transition is remarkably narrow for ZrB₁₂ samples, which is a clear indication of good quality samples. The transition temperature is consistent with the previously reported values for ZrB₁₂ (6.03 K) [10, 11, 12] and is comparable larger than that of ZrB₂ samples (5.5 K) [2]. Despite the fact

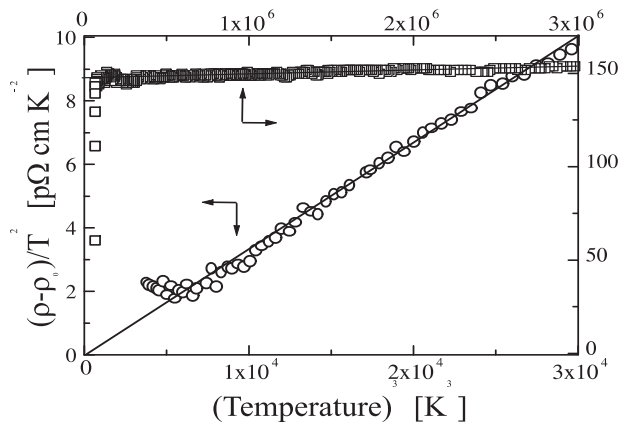


FIG. 4: Temperature dependence of the reduced resistivity $[\rho(T) - \rho(0)]/T^2$ of ZrB_{12} (open circles) and MgB_2 (squares) polycrystalline samples. The solid lines describe a guide for the eye.

that ZrB_{12} contains mostly boron, its room temperature resistivity is only four times larger than that of MgB_2 and ZrB_2 [2], while the residual resistivity is ten times larger. The resistivity ratio of ZrB_{12} ($R(300\text{ K})/R(6\text{ K}) \simeq 4$) is rather low compared to single crystal value 10 [23].

One can predict a nearly isotropic resistivity for *fcc* ZrB_{12} , which can be described by the Bloch-Grüneisen (BG) expression of the electron-phonon (*e-p*) scattering rate [24]:

$$\rho(t) - \rho(0) = 4\rho_1 t^5 \int_0^{1/t} \frac{x^5 e^x dx}{(e^x - 1)^2} = 4\rho_1 t^5 J_5(1/t) \quad (4)$$

Here, $\rho(0)$ is the residual resistivity, $\rho_1 = d\rho(T)/dt$ is a slope of $\rho(T)$ at high T ($T \gg T_R$), $t = T/T_R$, T_R is the resistive Debye temperature. As we can see from Fig. 3, the BG equation describes our data reasonably well, indicating the importance of electron-phonon interaction for both metals. The best fit to our data is obtained with $T_R = 270\text{ K}$ and 900 K for ZrB_{12} and MgB_2 , respectively.

In contrast to ZrB_{12} , the resistivity of MgB_2 samples does deviate from the BG model at low temperatures Eq. (4). This problem has been under consideration by several groups. In particular, Putti *et al.* [25] modified the BG equation introducing variable power n for the $t^n J_n(1/t)$ term in Eq. (4). The best fit to the data was obtained with $n = 3$ which in fact ignores a small angle *e-p* scattering. Recently Sologubenko *et al.* [26] reported a cubic T dependence in the *a, b* plane resistivity below 130 K in the single crystals of MgB_2 . This was attributed to the interband *e-p* scattering in transition metals.

We would like to stress that there are strong objections to this modified BG model: (i) a cubic $\rho(T)$ dependence is a theoretical model for large angle *e-p* scattering and no evidence of it was observed in transition and non-transition metals; (ii) numerous studies of the $\rho(T)$ dependence in transition metals have been successfully

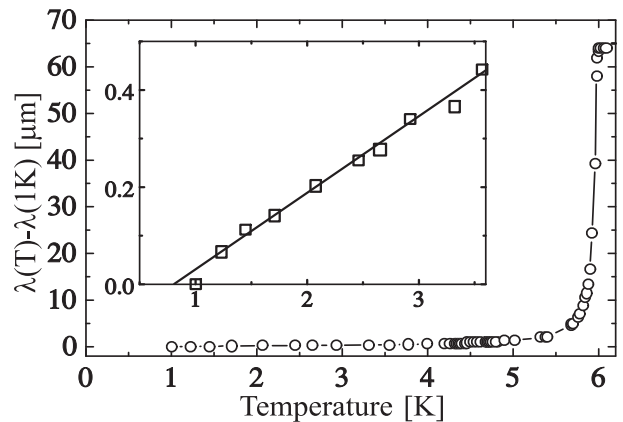


FIG. 5: Temperature dependence of the penetration depth for a ZrB_{12} sample. The solid lines describe a guide for the eye. The inset shows the data below 3.5 K in an extended scale.

described by a sum of electron-electron (*e-e*), T^2 , and *e-p*, T^5 , contributions to the low T resistivity, which may be easily confused with a T^3 law [24, 27, 28]; (iii) the interband $\sigma - \pi$ *e-p* scattering plays no role in normal transport in the two band model for MgB_2 [29].

To investigate whether combination of *e-e* and *e-p* scattering works for our samples we decided to add T^2 term to Eq. (4) [27, 28]. Note that the BG term is proportional to T^5 at low temperatures. Therefore, addition of the T^2 term results in the following expression for the resistivity $\rho(T)$:

$$[\rho(T) - \rho(0)]/T^2 = \alpha + \beta T^3 \quad (5)$$

Here α and β are parameters of *e-e* and *e-p* scattering terms, respectively. When plotted in $[\rho(T) - \rho(0)]/T^2$ vs T^3 axis such dependence yields a straight line with slope β and its y -intercept ($T = 0$) equal to α . Corresponding plot of our data in Fig. 4 clearly displays expected linear dependencies. Presence of unusually large T^2 term in MgB_2 data (open squares in Fig. 4) below 150 K is evident ($\alpha = 150\text{ p}\Omega\text{cm}/\text{K}^2$), whereas electron-phonon T^5 term is substantially smaller, ($\beta = 2.1 \times 10^{-6}\text{ p}\Omega\text{cm}/\text{K}^5$). One should also note that α value for MgB_2 is almost 40 times larger than corresponding values in transition metals such as molybdenum and tungsten ($\alpha_{Mo} = 2.5\text{ p}\Omega\text{cm}/\text{K}^2$ and $\alpha_W = 1.5 - 4\text{ p}\Omega\text{cm}/\text{K}^2$ [27, 28]). In contrast ZrB_{12} data display nearly zero T^2 term.

In general, there are many scattering processes responsible for the T^2 term in $\rho(T)$ of metals [23]. In particular, umklapp *e-e* scattering strongly contributes to this term. Furthermore normal collisions are significant in compensated metals and in thermal resistivity [28]. Borides have rather high T_R which depresses the *e-p* scattering, so that the *e-e* term is easier to observe. Clearly there is no obvious explanation for such strong *e-e* scattering contribution in MgB_2 . We believe additional experiments on the

more pure samples are necessary, before final conclusion about the origin of the T^2 term in $\rho(T)$ of MgB_2 can be drawn. Besides, the T^2 term was recently observed in ZrB_{12} single crystal samples with larger resistivity ratio of 10 [23]. Apparently, the T^2 term is residual resistivity dependent.

IV. Penetration Depth

Our RF technique allows us to measure the change in the penetration depth $\lambda(T)$ [22]. One should note however that there is some uncertainty in determining the absolute values of $\lambda(T)$ for bulk samples because of error in determination of the $f(0)$ in Eq. (2). For this reason, we do not attempt to determine the absolute values of $\lambda(0)$ for polycrystalline samples from these data but rather the temperature dependent part, $\Delta\lambda(T) = \lambda(T) - \lambda(1K)$. Fig. 5 displays the effect of superconducting transition in ZrB_{12} on $\lambda(T)$. The striking feature of the Fig. 5 curves is the linear temperature dependence of $\Delta\lambda(T)$ below $T_c/2 = 3K$. We should emphasize that no frequency dependence of these data was found when oscillator frequency was varied by two times.

In the BCS theory, the London penetration depth, $\lambda(T, l)$, is identical to the magnetic penetration depth $\lambda(T)$ for the case of specular and diffuse surface scattering and for negligible nonlocal effects, i.e. for $\delta(T, l) \gg \xi(T, l)$ [22, 30]. Here l - is the mean free path of carriers and ξ is the coherence length. In BCS-type superconductor (conventional *s-wave* pairing) in a clean-limit ($l \gg \xi$), the $\lambda(T)$ has an exponentially vanishing temperature dependence below $T_c/2$ (where $\Delta(T)$ is almost constant) [30]:

$$\lambda(T) = \lambda(0) \cdot \left[1 + \sqrt{\pi} \frac{\Delta(0)}{2k_B T} \times \exp\left(-\frac{\Delta(0)}{k_B T}\right) \right], \quad (6)$$

Here $\Delta(0)$ is the value of the energy gap and $\lambda(0)$ is a magnetic penetration depth at zero temperature.

At the same time, the unconventional *d-wave* pairing symmetry causes the energy gap to be suppressed along node lines on the Fermi surface. The latter results in a linear dependence of $\lambda(T) - \lambda(0) \propto T$ at low temperatures. Such a linear T dependence of the $\lambda(T)$ was currently used as a fingerprint of *d-wave* symmetry for Cooper pairs in cuprate superconductors [31, 32]. From this point, one could argue that the linear $\lambda(T)$ dependence in ZrB_{12} (Fig. 5) may be considered as indication of *d-wave* symmetry of Cooper pairs condensate.

Recently, however, thermodynamic arguments were suggested [33], that a strictly linear T dependence of $\lambda(T)$ at low temperatures violates the third law of thermodynamics, since it produces the non vanished entropy in the zero temperature limits. Therefore one should expect a deviation from the linear T dependence of $\lambda(T)$ at very low temperatures. Indeed, recent experiments in cuprates indicate deviation from the linearity of $\lambda(T)$ from current carrying zero energy surface Andreev bound

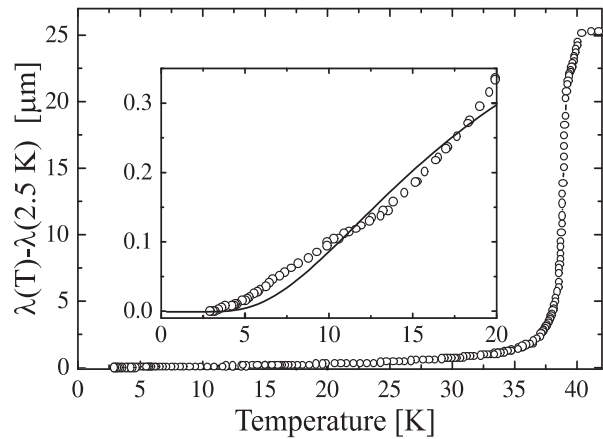


FIG. 6: Temperature variation of the magnetic penetration depth, $\lambda(T)$, for MgB_2 sample up to T_c . The inset shows the data below $T_c/2$ on an extended scale. The solid line represents the single gap exponential fit for $\Delta(0) = 2.73 \text{ meV}$.

states [34]. We believe that further experiments on single crystals of ZrB_{12} are necessary to confirm actual character of the $\lambda(T)$ behavior below 1.0 K. Such experiments are in progress and may shed light on the nature of pairing state in this dodecaboride.

Fig. 6 displays the change in $\lambda(T)$ in MgB_2 polycrystalline sample. These measurements were done on samples freely placed in rectangular solenoid coil forming LC circuit which was kept at 2.5 K. In Fig. 7 we show the temperature variation of $\lambda(T)$ for the best MgB_2 film as determined from one-coil technique and inversion procedure by use of Eq. (2). A particular feature of these figures is a very similar exponential T dependence at low temperatures for both film and polycrystalline samples. We used conventional *s-wave* approach Eq. (6) to fit these data. In both case we observe satisfactory if not perfect agreement between the fits and low temperature data for thin films. Our fitting parameters (superconducting gap value at 0K) are 2.8 meV and 2.73 meV, for film and polycrystalline samples respectively. Corresponding reduced gap $2\Delta(0)/k_B T_c$ for these samples was found to be 1.64 and 1.62.

Several recent reports on $\lambda(T)$ measurements [21, 35] in MgB_2 provide strong evidence for a predominately exponential temperature dependence of $\lambda(T)$ at low temperatures, which is consistent with our observation. The reduced gap deduced from exponential fits to the data was found to be 1.42 [35] and 2.3 [21] for single crystals and thin films respectively. These values, as well as the value we obtained from our data, are significantly smaller than the BCS weak coupling value $2\Delta(0)/k_B T_c = 3.52$. Several other groups have claimed that $\lambda(T)$ in MgB_2 does follow a power law or even linear T dependence [36]. The possible reason for this discrepancy is that previous studies have been limited to temperatures above 4 K, whereas $\lambda(T)$ shows a clear signature of exponential behavior only below 7 K (see Fig. 6 and Fig. 7). Another

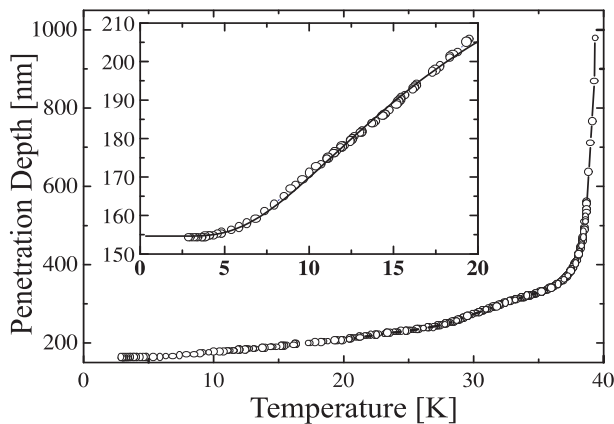


FIG. 7: Temperature variation of $\lambda(T)$ up to T_c for an MgB_2 thin film on Al_2O_3 . The inset shows the data below $T_c/2$ on extended scale. The solid line represents the single gap exponential fit for $\Delta(0) = 2.8\text{meV}$.

problem may arise in use of non etched samples where the damaged surface layer or the proximity effect, associated with the presence of a metallic Mg overlayer [17], may significantly complicate the use of the surface sensitive techniques.

We would like to emphasize that our value of the superconducting gap at low T are in the range of values for 3D π - bands obtained by point-contact spectroscopy on MgB_2 single crystals ($\Delta_\sigma = 7.1\text{meV}$ and $\Delta_\pi = 2.9\text{meV}$ for the σ and π bands, respectively) [37]. Our data also agree with the theoretical values predicted by the two-band model [38]. Analysis of overall temperature dependence of $\lambda(T)$ dependence by aid of a two band phenomenological model [39] is in progress now and will be published elsewhere. The essential property of this paper is comparison a ZrB_{12} and MgB_2 low temperature data, where $\lambda(T)$ dependence has completely different behavior.

V. Upper Critical Magnetic Field

We now turn to the data on electronic transport in magnetic field. Fig. 8 presents the magnetic field dependent electrical resistivity data for a ZrB_{12} polycrystalline samples at various temperatures. Two features are clearly seen: (i) magnetic field shifts the superconducting transition to lower temperatures, (ii) there is a very small magnetoresistivity in the normal state. We extracted completion upper critical magnetic field H_{c2} by extending the maximal derivative $d\rho/dH$ line (dashed line in Fig. 8) up to the normal state level. The crossing point of this line and normal state resistivity gave us the value of H_{c2} at various temperatures as indicated by arrow in Fig. 8. Despite a clear broadening at higher fields, such onset of resistive transition remains well defined. One should note however that the resistance may not be an intrinsic property and may be related to the poor grain connection in our polycrystalline samples. Therefore, to get a better test for the onset of the superconducting

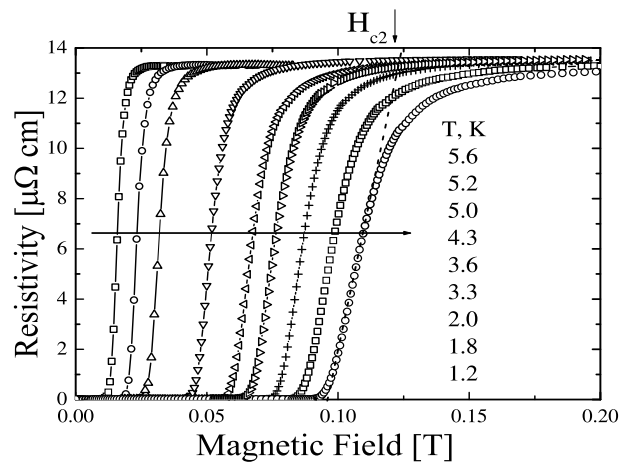


FIG. 8: Magnetic field variation of the resistivity $\rho(T)$ in linear scale for a ZrB_{12} sample. The solid lines describe a guide for the eye and the dashed line describes how the resistive transition H_{c2} has been established.

transition we measured RF susceptibility.

Figure 9 shows a plot of the temperature dependence of the resonant frequency of our LC circuit, $f(T)$, as a function of longitudinal magnetic field. The set-up of the sample arrangement is shown on an inset in the Fig. 9. Changes in the resonant frequency are directly proportional to the RF susceptibility of the sample. To deduce the $H_{c2}(T)$, we used a straight-line fit representing the maximum of derivative df/dH (dashed line in Fig. 9). This straight line was extended up to normal state frequency values. We defined H_{c2} as an crossing point of this line with normal state frequency $f(T)$. As we can see from Fig. 9, this point is very close to the onset point of $f(T)$ in this plot, that makes determination of $H_{c2}(T)$ more reliable.

Figure 10 presents the $H_{c2}(T)$ data that we deduced from these two techniques. A remarkable feature of this plot is the near linear increase of H_{c2} with decreasing temperature for both data with no evidence of saturation down to 1.1K . To obtain the value of $H_{c2}(0)$ from our RF data we assumed that $H_{c2}(0) = 0.71T_c dH_{c2}/dT$ [40] at zero temperature. This assumption yields $H_{c2}(0) = 0.11\text{ T}$, which is substantially smaller than the extrapolated value 0.15 T . Nevertheless, we used this number to obtain the coherence length $\xi(0)$, by employing the relations $H_{c2}(0) = \phi_0/2\pi\xi^2(0)$. The latter yields $\xi(0) = 60.3\text{ nm}$, the value which is substantially larger than a few angstroms coherence length of high- T_c superconductors. The accuracy of our measurements of $\lambda(T)$ in ZrB_{12} did not allow us to determine the absolute values of $\lambda(0)$. Therefore, the Ginzburg-Landau parameter, $\kappa = \lambda/\xi$ could not be determined from the measurements.

Taken as a whole, the temperature dependence of $H_{c2}(T)$ for ZrB_{12} is very similar to that found in MgB_2 [41, 42] and BaNbO_x [43] compounds. Unlike conventional BCS theory [40], $H_{c2}(T)$ is linear over an extended region of temperatures with no evidence of saturation

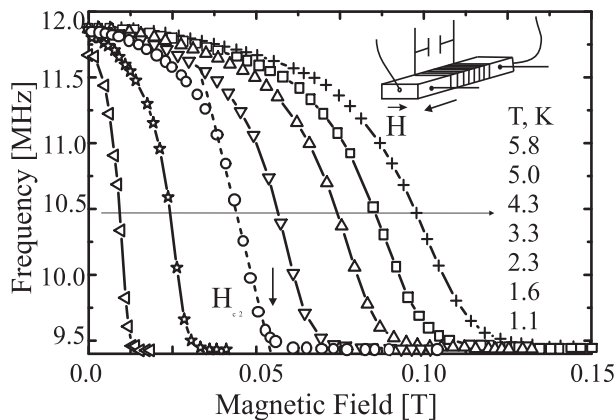


FIG. 9: Magnetic field variation of the resonant frequency of LC circuit for an ZrB_{12} sample, at different temperatures. The solid lines are guide to the eye and the dashed line describes a linear extrapolation of the RF data used for $H_{c2}(T)$ determination.

at low T . Although the origin of this feature is not completely understood, similar linear $H_{c2}(T)$ dependence have been observed in other high borides and oxide compounds [41, 42, 43].

VI. Conclusions

We successfully performed syntheses of polycrystalline samples of dodecaboride ZrB_{12} and diboride MgB_2 . We systematically studied the temperature dependence of resistivity, $\rho(T)$, the magnetic penetration depth, $\lambda(T)$, and upper critical magnetic field, $H_{c2}(T)$, in these compounds. The electron transport and superconducting properties have been compared with aim to shade light on the origin of superconductivity in borides. Although a standard Bloch-Grüneisen expression describes the resistivity data fairly well in ZrB_{12} , better fit was obtained by adding electron-electron scattering T^2 term in $\rho(T)$ of MgB_2 . This square term dominates the $\rho(T)$ dependence below 150 K in MgB_2 , though is almost zero for ZrB_{12} .

The temperature dependence of $\lambda(T)$ of both polycrystalline and thin film MgB_2 samples is well described by a s -wave behavior of the order parameter symmetry. Our value of the reduced superconducting gap in MgB_2 samples ($2\Delta(0)/k_B T_c = 1.6$) is significantly smaller than the weak coupling BCS value. However this value is in a very good agreement with other direct probe measurements of smaller gap - on the π - sheets of the Fermi surface. At the same time, we find that $\lambda(T)$ in ZrB_{12} has linear tem-

perature dependence over an extended region of T . This feature may be indicative of the d -wave pairing. We find that the $H_{c2}(T)$ deduced from RF data is almost the same as an that obtained from the resistive data. Both techniques demonstrate unconventional linear temperature dependence of the $H_{c2}(T)$, with a considerably lower value of $H_{c2}(0) = 0.15$ T. We believe that these observations are clear indicators of the unconventional behavior of electron transport and superconducting properties of

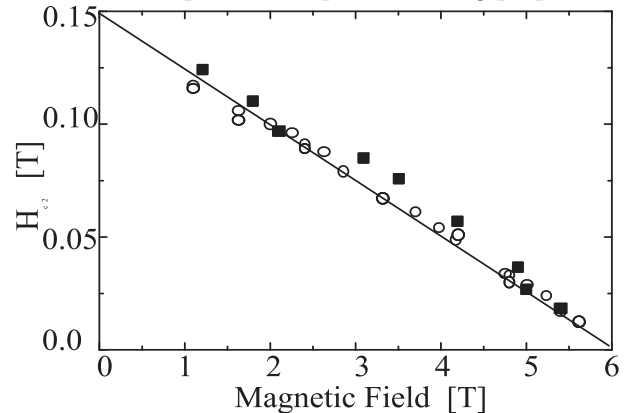


FIG. 10: Temperature variation of upper critical magnetic field of ZrB_{12} sample. Different symbols represent the data determined from $\rho(H)$ (squares) and $f(H)$ (circles) data as described in text.

dodecaboride ZrB_{12} .

Acknowledgments

Very useful discussion with V.F. Gantmakher, A.A. Golubov, A. Junod, H. Hilgenkamp, R. Huguenin, help in samples preparation from V.V. Lomejko and help in text preparation of L.V. Gasparov, are gratefully acknowledged. Many thanks to H.M. Christen, H.-Y. Zhai, M. Paranthaman, and D.H. Lowndes for preparation of excellent MgB_2 films. This work was supported by the Russian Scientific Programs: Superconductivity of Mesoscopic and Highly Correlated Systems (Volna 4G); Synthesis of Fullerenes and Other Atomic Clusters (No.541-028); Surface Atomic Structures (No.4.10.99), Russian Ministry of Industry, Science and Technology (MSh-2169.2003.2), RFBR (No.02-02-16874-a) and by the INTAS (No.01-0617).

-
- [1] J. Nagamatsu, N. Nakagawa, T. Muranaka, Y. Zanitani, and J. Akimitsu, *Nature* **410**, 63 (2001).
 - [2] V.A. Gasparov, N.S. Sidorov, I.I. Zver'kova, M.P. Kulakov, *JETP Letters* **73**, 601 (2001).
 - [3] Z. Fisk, *AIP Conf. Proc.* **#231** (1991).
 - [4] D.P. Young, R.G. Goodrich, P.W. Adams, J.Y. Chan,

- F.R. Fronczek, F. Drymiotis, and L.L. Henry, *Phys. Rev.* **B65**, 180518(R) (2002).
- [5] D. Kaczorowski, A.J. Zaleski, O.J. Zogal, J. Klamut, *cond-mat/0103571* (2001); D. Kaczorowski, J. Klamut, A.J. Zaleski, *cond-mat/0104479* (2001).
- [6] H. Rosner, W.E. Pickett, S.-L. Drechsler, A. Handstein,

- G. Behr, G. Fuchs, K. Nenkov, K.-H. Müller, and H. Eschrig, *Phys.Rev.* **B64**, 144516 (2001).
- [7] N. Ashcroft, *Phys. Rev. Lett.* **21**, 1748 (1968).
- [8] J. Kortus, I.I. Mazin, K.D. Belashchenko, V.P. Antropov, L.L. Boyer, *Phys. Rev. Lett.* **86**, 4656 (2001).
- [9] M.L. Eremets, V.V. Struzhkin, H.K. Mao, R.J. Hemley, *Science* **203**, 272 (2001).
- [10] B.T. Matthias, T.H. Geballe, K. Andres, E. Corenzwit, G. Hull, J.P. Maita, *Science*, **159**, 530 (1968).
- [11] C.W. Chu and H.H. Hill, *Science* **159**, 1227 (1968).
- [12] Z. Fisk, A.C. Lawson, B.T. Matthias and E. Corenzwit, *Phys. Lett.* **37A**, 251 (1971).
- [13] K. Hamada, M. Wakata, N. Sugii, K. Matsuura, K. Kubo, and H. Yamauchi, *Phys. Rev.* **B 48**, 6892 (1993).
- [14] I.R. Shein and A.L. Ivanovskii, *Physics of the Solid State* **45**, 1429 (2003); [*Fizika Tverdogo Tela* **45**, 1363 (2003)].
- [15] A. Leithe-Jasper, A. Sato, T. Tanaka, et al., *NCS* **217**, 319 (2002).
- [16] I.R. Shein, N.I. Medvedeva, and A.L. Ivanovskii, *Physics of the Solid State* **45**, 1617 (2003), [*Fizika Tverdogo Tela* **45**, 1541 (2003)].
- [17] M. Paranthaman, C. Cantoni, H.Y. Zhai, H.M. Christen, T. Aytug, S. Sathyamurthy, E.D. Specht, J.R. Thompson, D.H. Lowndes, H.R. Kerchner, and D.K. Christen, *Appl. Phys. Lett.* **78**, 3669 (2001).
- [18] V.A. Gasparov and A.P. Oganessian, *Physica C* **178**, 445 (1991).
- [19] A. Gauzzi, J. Le Cochee, G. Lamura, B.J. Jönsson, V.A. Gasparov, F.R. Ladan, B. Placais, P.A. Probst, D. Pavuna, J. Bok, *Rev. Sci. Instr.* **71**, 2147 (2000).
- [20] V.A. Gasparov, I. Batov, Qi Li, and C. Kwon, *Physica B* **284-288**, 1021 (2000); *Czechoslovak J. Phys.* **46** (Suppl. S3) 1401 (1996); *Proc. SPIE* 2697, 391(1996); *Phys. of Low-Dim. Str.*, **6**, n.12, 36 (1995); V.A. Gasparov, G. Tsydynzhapov, I.E. Batov and Qi Li, *J. Low Temp. Phys.*, (to be published, 2004).
- [21] G. Lamura, E. Di Gennaro, M. Salluzzo, A. Andreone, J. Le Cochee, A. Gauzzi, C. Cantoni, M. Paranthaman, D.K. Christen, H.M. Christen, G. Giunchi and S. Ceresara, *Phys. Rev.* **B 65**, 020506 (2002).
- [22] V.A. Gasparov, M.R. Mkrtychyan, M.A. Obolensky, A.V. Bondarenko, *Physica C* **231**, 197 (1994).
- [23] V.A. Gasparov, M.P. Kulakov, N.S. Sidorov, I.I. Zver'kova, V.B. Filipov, A.B. Lyashenko, Yu.B. Paderno, *JETP Letters* **80**, 330 (2004) [*Pis'ma v ZhETF* **80**, 376 (2004)].
- [24] J.M. Ziman, *Electrons and Phonons, Theory of Transport Phenomena in Solids* (Oxford U.P., Oxford, England, 1960).
- [25] M. Putti, E.G. d'Agliano, D. Marré, F. Napoli, M. Tassisto, P. Manfrinetti, A. Palenzona, C. Rizzuto, S. Masidda, *Eur. Phys. J. B* **25**, 439 (2002).
- [26] A.V. Sologubenko, J. Jun, S. M. Kazakov, J. Karpinski, and H. R. Ott, *Phys. Rev.* **B 66**, 014504 (2002).
- [27] N.V. Vol'kenshtein, V.P. Dyakina, V.E. Startsev, *phys. stat. sol.* **57**, 9 (1973).
- [28] V.A. Gasparov and R. Huguenin, *Adv. Phys.*, **42**, 393 (1993).
- [29] I.I. Mazin, O.K. Andersen, O. Jepsen, O. V. Dolgov, J. Kortus, A. A. Golubov, A. B. Kuz'menko, and D. van der Marel, *Phys. Rev. Lett.* **89**, 107002 (2002).
- [30] J. Halbritter, *Z. Phys.* **243**, 201 (1971).
- [31] W.N. Hardy, D.A. Bonn, D.C. Morgan, R. Liang, and K. Zhang, *Phys. Rev. Lett.* **70**, 3999 (1993).
- [32] D.A. Bonn, S. Kamal, K. Zhang, R. Liang, D.J. Baar, E. Klein, and W.N. Hardy, *Phys. Rev.* **B 50**, 4051 (1994).
- [33] N. Schopohl and O.V. Dolgov, *Phys. Rev. Lett.* **80**, 4761 (1998); *Ibid* **81**, 4025 (1998).
- [34] A. Carrington, F. Manzano, R. Prozorov, R.W. Giannetta, N. Kameda, and T. Tamegai, *Phys. Rev. Lett.* **86**, 1074 (2001).
- [35] F. Manzano, A. Carrington, N.E. Hussey, S. Lee, A. Yamamoto, and S. Tajima, *Phys. Rev. Lett.* **88**, 047002 (2002).
- [36] Yu.A. Nefyodov, M.R. Trunin, A.F. Shevchun, D.V. Shovkun, N.N. Kolesnikov, M.P. Kulakov, A. Agliolo Gallitto and S. Fricano, *Europhysics Letters*, **58**, 422 (2002).
- [37] R.S. Gonnelli, D. Daghero, G.A. Ummarino, V.A. Stepanov, J. Jun, S.M. Kazakov and J. Karpinski, *Phys. Rev. Lett.* **89**, 247004 (2002).
- [38] A. Brinkman, A.A. Golubov, H. Rogalla, O.V. Dolgov, J. Kortus, Y. Kong, O. Jepsen, and O.K. Andersen, *Phys. Rev.* **B 65**, 180517(R) (2001); A.A. Golubov, A. Brinkman, O.V. Dolgov, J. Kortus, and O. Jepsen, *Phys. Rev.* **B 66**, 054524(2002).
- [39] F. Bouquet, Y. Wang, R.A. Fisher, D.G. Hinks, J.D. Jorgensen, A. Junod, and N.E. Phillips, *Europhys. Lett.* **56**, 856 (2001).
- [40] E. Helfand and N.R. Werthamer, *Phys. Rev. Lett.* **13**, 686 (1964); *Phys. Rev.* **147**, 288 (1966).
- [41] L. Lyard, P. Samuely, P. Szabo, T. Klein, C. Marcenat, L. Paulius, K. H. P. Kim, C.U. Jung, H.-S. Lee, B. Kang, S. Choi, S.-I. Lee, J. Marcus, S. Blanchard, A.G. M.Jansen, U. Welp, G. Karapetrov, and W.K. Kwok, *Phys. Rev.* **B 66**, 180502 (R) (2002).
- [42] A.V. Sologubenko, J. Jun, S.M. Kazakov, J. Karpinski, and H.R. Ott, *Phys. Rev.* **B 66**, 180505(R) (2002).
- [43] V.A. Gasparov, S.N. Ermolov, S.S. Khasanov, G.K. Strukova, L.V. Gasparov, H.-S. Wang, Qi Li, M. Schneider, Wo. Richter, E. Glaser, F. Schmidl, P. Seidel, B.L. Brandt, *Physica B*, **284-288**, 1119 (2000).